Structural Engineering and Mechanics, *Vol. 71, No. 3 (2019) 245-255*
DOI: https://doi.org/10.12989/sem.2019.71.3.245

Numerical study on the walking load based on inverted-pendulum model

Liang Cao*[1, 2], Jiepeng Liu[1, 2a], Xiaolin Zhang[1, 2b] and Y. Frank Chen[1, 2a]

[1]*School of Civil Engineering, Chongqing University, Chongqing 400045, China*
[2]*Key Laboratory of New Technology for Construction of Cities in Mountain Area (Chongqing University), Ministry of Education, Chongqing 400045, China*

(Received November 26, 2018, Revised March 30, 2019, Accepted April 1, 2019)

Abstract. In this paper, an inverted-pendulum model consisting of a point supported by spring limbs with roller feet is adopted to simulate human walking load. To establish the kinematic motion of first and second single and double support phases, the Lagrangian variation method was used. Given a set of model parameters, desired walking speed and initial states, the Newmark-β method was used to solve the above kinematic motion for studying the effects of roller radius, stiffness, impact angle, walking speed, and step length on the ground reaction force, energy transfer, and height of center of mass transfer. The numerical simulation results show that the inverted-pendulum model for walking is conservative as there is no change in total energy and the duration time of double support phase is 50-70% of total time. Based on the numerical analysis, a dynamic load factor α_{wi} is proposed for the traditional walking load model.

Keywords: inverted-pendulum model; walking load; newmark-β method; ground reaction force; dynamic load factor

1. Introduction

With the rapid advancement in material technology, structural design and construction techniques, the exploration of a more light-weight and slender structural form has become a trendy development in structural engineering world. Consequently, the human-induced vibration serviceability has drawn an increasing attention due to the potential annoyance (Ahmadi *et al*. 2018; Cao *et al*. 2018; Chen *et al*. 2013; Liu *et al*. 2019; Setareh 2016; Van Nimmen *et al*. 2017). Numerical simulation, theoretical analysis, and experimental study are the primary means for studying serviceability issues, especially the first two methods (Davis and Avci 2015, Petrovic-Kotur and Pavic 2016; Yin *et al*. 2017; Zhou *et al*. 2017). The accuracy of the human-induced load will undoubtedly affect vibration analysis results regardless of the research tool used. Among the reported human-induced loads, walking being the most common human activity appears to much higher (Brownjohn *et al*. 2018; Kim and Jeon 2014; Mello *et al*. 2008; Wang and Chen 2017).

Several walking load models based on the probability statistics have been proposed and investigated by various researchers. For example, Blanchard *et al*. (1977) and Smith *et al*. (2009) suggested a simple harmonic walking load $F_w(t)$ as expressed in Eq. (1)

$$F_w(t) = G\sum_{i=1}^{n}\alpha_{wi}\sin(2i\pi f_w t - \theta_{wi}) \quad (1)$$

Table 1 Load parameters of the various available walking models

Scholar	α_{wi}	θ_{wi}	G	f_w
Blanchard	α_{wi}=0.257	---	700	---
Bachmann & Ammann	α_{wi}=0.4, f_w=2.0 α_{wi}=0.4, f_w=2.4 α_{w2}=α_{w3}=0.1, f_w=2.0	θ_{w1}=0 θ_{w2}=π/2 θ_{w3}=π/2	---	2.0-2.4
Rainer *et al*.	Fig. 1	---	735	1.7-2.3
Allen & Murray *et al*.	α_{w1}=0.5 α_{w2}=0.2 α_{w3}=0.1 α_{w4}=0.05 α_{w1}=-0.265f_w^3+1.321f_w^2	θ_{w1}=0 θ_{w2}=0 θ_{w3}=0 θ_{w4}=0		1.6-2.2
Kerr	-1.760f_w+0.761 α_{w2}=0.07 α_{w3}=0.05	---	---	1.6-2.2
Smith *et al*.	α_{w1}=0.436(f_w-0.95) α_{w2}=0.006(2f_w+12.3) α_{w3}=0.007(3f_w+5.2) α_{w4}=0.007(4f_w+2.0)	θ_{w1}=0 θ_{w2}=π/2 θ_{w3}=π θ_{w4}=π/2	746	1.8-2.2
Chen *et al*.	α_{w1}=0.2358f_w-0.2010 α_{w2}=0.0949 α_{w3}=0.0523 α_{w4}=0.0461 α_{w5}=0.0339	θ_{w1}=-π/4 θ_{w2}=0 θ_{w3}=0 θ_{w4}=π/4 θ_{w5}=π/2	---	1.2-3.0

where α_{wi} (i=1) is the dynamic load factor (DLF), G is the person's weight (N), and f_w is the walking frequency (Hz). Bachmann and Ammann (1987), Rainer *et al*. (1988), Allen and Murray (1993), Murray *et al*. (1997, 2016), Kerr (1998), and Chen (2014) reported the following load model:

$$F_w(t) = G[1+\sum_{i=1}^{n}\alpha_{wi}\sin(2i\pi f_w t - \theta_{wi})] \quad (2)$$

*Corresponding author, Postdoctor
E-mail: liangcao@cqu.edu.cn
[a] Professor
[b] M.Sc. Candidate

ISSN: 1225-4568 (Print), 1598-6217 (Online)

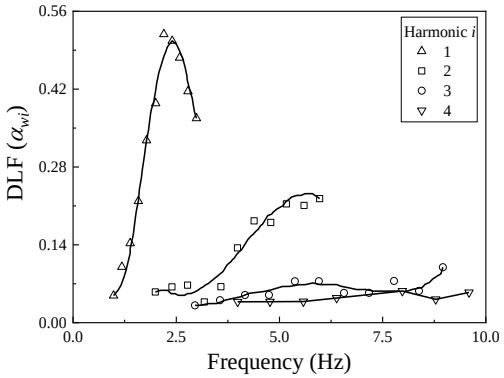

Fig. 1 The recommended DLFs values by Rainer *et al.* (1988)

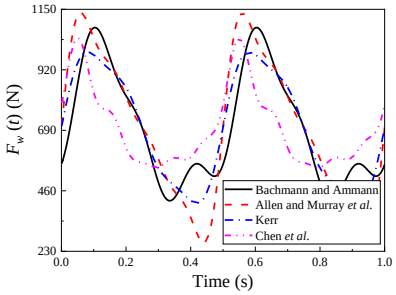

Fig. 2 Comparison of available walking loads (G=700N)

where n is the order of the function, and θ_{wi} is the phase angle of the ith harmonic (rad). Table 1 lists the DLFs (α_{wi}) along with θ_{wi}, G and f_w values.

Comparing the synthesized load time with the same walking frequency f_w=2Hz, Fig. 2 reveals a significant difference in the acceleration responses predicted by the different walking models, resulting in an inaccurate evaluation on vibration serviceability, especially the human-structure interaction issue (Bocian *et al.* 2014; Han *et al.* 2017; Liu *et al.* 2019; Setareh and Gan, 2018). Moreover, the above walking load models ignore the difference in gaits from different individuals. So, establishing a more appropriate walking load model to avoid the above-mentioned deficiencies is the focus of this paper. The inverted-pendulum model (also known as mass-spring model with roller feet) suggested by Whittington and Thelen (2009) was adopted to study the walking load numerically. The scope of this research is summarized as follows: Firstly, the kinematic motion of the first/second single- and double- support phases are derived using the Lagrangian formulation; Secondly, the vertical and horizontal ground reaction forces are established; Thirdly, Newmark-β method was used to solve the above kinematic motion for studying the effect of roller radius, stiffness, impact angle, and walking speed on the ground reaction force, energy transfer, height of center of mass transfer, and step length; and Finally, a dynamic load factor α_{wi} is proposed for the traditional walking load model.

2. Kinematic motion

The whole walking process includes three stages, i.e. first single-support, double-support and second single-support (Refer to section 4). In this section, the focus is the derivation of the kinematic motion of each stage.

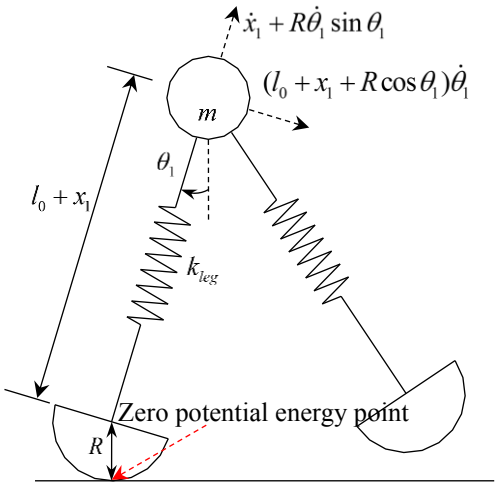

Fig. 3 First single-support phase

2.1 First and second single support

The kinematic motion of the inverted-pendulum model (Fig. 3) for the first single-support was derived using Lagrangian formulation. The total system potential energy V (i.e., Eq. (3)) includes the elastic energy stored in the springs and the gravitational energy associated with the height of the mass m

$$V = \frac{1}{2}k_{leg}x_1^2 + mg[(l_0 + x_1)\cos\theta_1 + R] \tag{3}$$

where k_{leg} is the spring stiffness, $x_1(t)$ is the spring compression, l_0 is the unstretched spring length, R is the roller radius, m is the point mass, g is the gravitational constant, and $\theta_1(t)$ is the inclination of the limb (Fig. 3).

The velocity $\vec{v}$ (i.e. Eq. (4)) of the point mass can be conveniently expressed via components directed both radial velocity ($\vec{e}_{l_0+x_1}$) and circumferential velocity ($\vec{e}_{\theta_1}$)

$$\vec{v} = (\dot{x}_1 + R\dot{\theta}_1\sin\theta_1)\vec{e}_{l_0+x_1} + (l_0 + x_1 + R\cos\theta_1)\dot{\theta}_1\vec{e}_{\theta_1} \tag{4}$$

where "$\cdot$" indicates a derivative with respect to time. The total system kinetic energy T is thus given by

$$T = \frac{1}{2}m[(l_0 + x_1 + R\cos\theta_1)^2\dot{\theta}_1^2 + (\dot{x}_1 + R\dot{\theta}_1\sin\theta_1)^2] \tag{5}$$

The potential and kinetic energy expressions can be combined to form the Lagrangian $\mathcal{L} = T - V$, which is a function of $x_1(t)$ and $\theta_1(t)$

$$\begin{aligned}\mathcal{L} = T - V = \frac{1}{2}m[&(l_0^2 + x_1^2 + R^2 + 2l_0x_1 + 2l_0R\cos\theta_1 \\ &+2Rx_1\cos\theta_1)\dot{\theta}_1^2 + \dot{x}_1^2 + 2R\dot{x}_1\dot{\theta}_1\sin\theta_1] - \frac{1}{2}k_{leg}x_1^2 \\ &-mg[(l_0 + x_1)\cos\theta_1 + R]\end{aligned} \tag{6}$$

The Lagrangian equations of motion are given by

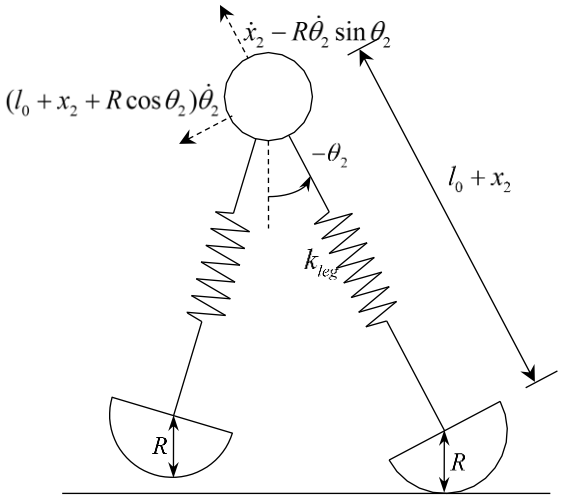

Fig. 4 Second single-support phase

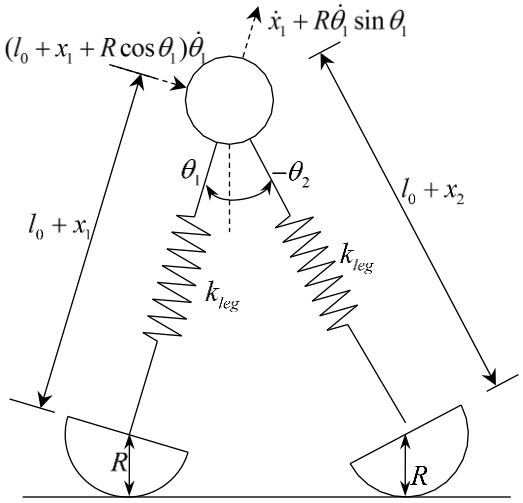

Fig. 5 Double support phase

$$\frac{d}{dt}\left(\frac{\partial \mathcal{L}}{\partial \dot{x}_1}\right) - \frac{\partial \mathcal{L}}{\partial x_1} = 0 \tag{7}$$

$$\frac{d}{dt}\left(\frac{\partial \mathcal{L}}{\partial \dot{\theta}_1}\right) - \frac{\partial \mathcal{L}}{\partial \theta_1} = 0 \tag{8}$$

Substituting Eq. (6) into Eqs. (7) and (8) gives the kinematic motion

$$\ddot{x}_1 + R\ddot{\theta}_1 \sin\theta_1 - (l_0 + x_1)\dot{\theta}_1^2 + \omega_1^2 x_1 + g\cos\theta_1 = 0 \tag{9}$$

$$\begin{aligned} &R\ddot{x}_1 \sin\theta_1 + [(l_0 + x_1)^2 + R^2 + 2(l_0 + x_1)R\cos\theta_1]\ddot{\theta}_1 \\ &+2(l_0 + x_1 + R\cos\theta_1)\dot{x}_1\dot{\theta}_1 - (l_0 + x_1)(g + R\dot{\theta}_1^2)\sin\theta_1 = 0 \end{aligned} \tag{10}$$

where $\omega_1^2 = k_{leg}/m$.

Similar to the first single-support, the kinematic motion of the second single-support phase (Fig. 4) can be written as

$$\begin{aligned} &\ddot{x}_2 - R\ddot{\theta}_2 \sin\theta_2 - (l_0 + x_2 + 2R\cos\theta_2)\dot{\theta}_2^2 \\ &+\omega_1^2 x_2 + g\cos\theta_2 = 0 \end{aligned} \tag{11}$$

$$\begin{aligned} &R\ddot{x}_2 \sin\theta_2 - [(l_0 + x_2)^2 + R^2 + 2(l_0 + x_2)R\cos\theta_2]\ddot{\theta}_2 \\ &-2(l_0 + x_2 + R\cos\theta_2)\dot{x}_2\dot{\theta}_2 \\ &+(l_0 + x_2)(g + R\dot{\theta}_2^2)\sin\theta_2 = 0 \end{aligned} \tag{12}$$

2.2 Double support phase

The total system potential energy V and kinetic energy T (Fig. 5) can be written as

$$V = \frac{1}{2}k_{leg}x_1^2 + \frac{1}{2}k_{leg}x_2^2 + mg[(l_0 + x_1)\cos\theta_1 + R] \tag{13}$$

$$T = \frac{1}{2}m[(l_0 + x_1 + R\cos\theta_1)^2\dot{\theta}_1^2 + (\dot{x}_1 + R\dot{\theta}_1\sin\theta_1)^2] \tag{14}$$

where $x_2(t)$ is the spring compression. So, the Lagrangian formulation $\mathcal{L} = T - V$ is

$$\begin{aligned} \mathcal{L} = T - V = \frac{1}{2}m[&(l_0^2 + x_1^2 + R^2 + 2l_0x_1 + 2l_0R\cos\theta_1 \\ &+2Rx_1\cos\theta_1)\dot{\theta}_1^2 + \dot{x}_1^2 + 2R\dot{x}_1\dot{\theta}_1\sin\theta_1] - \frac{1}{2}k_{leg}x_1^2 \\ &-\frac{1}{2}k_{leg}x_2^2 - mg[(l_0 + x_1)\cos\theta_1 + R] \end{aligned} \tag{15}$$

However, the system possesses only two independent degrees of freedom such that the angular velocity $\dot{\theta}_2$ and spring velocity $\dot{x}_2$ can be described in terms of the respective velocities $\dot{\theta}_1$ and $\dot{x}_1$. In the paper, no slip between either roller and the ground during contact is assumed. Consequently, the closed-loop kinematic constraints can be used to determine the function during the double support, as follows

$$\begin{aligned} \dot{x}_2 = &-\frac{(l_0 + x_2)\cos(\theta_1 - \theta_2) + R\cos\theta_1}{l_0 + x_2 + R\cos\theta_2}\dot{x}_1 \\ &-\frac{1}{l_0 + x_2 + R\cos\theta_2}[R(l_0 + x_2)\sin\theta_2 \\ &-(l_0 + x_1)(l_0 + x_2)\sin(\theta_1 - \theta_2) - R(l_0 + x_1)\sin\theta_1]\dot{\theta}_1 \end{aligned} \tag{16}$$

$$\begin{aligned} \dot{\theta}_2 = &\frac{\sin(\theta_1 - \theta_2)}{l_0 + x_2 + R\cos\theta_2}\dot{x}_1 \\ &+\frac{(l_0 + x_1)\cos(\theta_1 - \theta_2) + R\cos\theta_2}{l_0 + x_2 + R\cos\theta_2}\dot{\theta}_1 \end{aligned} \tag{17}$$

Differentiating Eqs (16) and (17) gives the following relationship for the acceleration of two limbs

$$\begin{aligned} \ddot{x}_2 = &-\frac{(l_0 + x_2)\cos(\theta_1 - \theta_2) + R\cos\theta_1}{l_0 + x_2 + R\cos\theta_2}\ddot{x}_1 \\ &-\frac{1}{l_0 + x_2 + R\cos\theta_2}[R(l_0 + x_2)\sin\theta_2 - (l_0 + x_1)(l_0 + x_2)\sin(\theta_1 - \theta_2) \\ &-R(l_0 + x_1)\sin\theta_1]\ddot{\theta}_1 - \frac{(l_0 + x_2)\sin^2(\theta_1 - \theta_2)}{(l_0 + x_2 + R\cos\theta_2)^2}\dot{x}_1^2 \end{aligned} \tag{18}$$

$$+\frac{1}{(l_0+x_2+R\cos\theta_2)^2}\{2R^2\sin\theta_1\cos\theta_2+(l_0+x_2)[2R\sin\theta_1$$
$$-(l_0+x_1)\sin(2\theta_1-2\theta_2)+2(l_0+x_2)\sin(\theta_1-\theta_2)]\}\dot{x}_1\dot{\theta}_1$$
$$+\frac{1}{(l_0+x_2+R\cos\theta_2)^2}\{(l_0+x_1)(l_0+x_2)[(l_0+x_2)\cos(\theta_1-\theta_2)$$
$$-R\sin(\theta_1-\theta_2)\sin\theta_2-(l_0+x_1)\cos^2(\theta_1-\theta_2)]$$
$$+R^2[(l_0+x_1)\cos\theta_1\cos\theta_2-\cos^2\theta_2]\}\dot{\theta}_1^2$$

$$\ddot{\theta}_2=\frac{\sin(\theta_1-\theta_2)}{l_0+x_2+R\cos\theta_2}\ddot{x}_1+\frac{(l_0+x_1)\cos(\theta_1-\theta_2)+R\cos\theta_2}{l_0+x_2+R\cos\theta_2}\ddot{\theta}_1$$
$$+\frac{2\cos(\theta_1-\theta_2)}{l_0+x_2+R\cos\theta_2}\dot{x}_1\dot{\theta}_1-\frac{(l_0+x_1)\sin(\theta_1-\theta_2)}{l_0+x_2+R\cos\theta_2}\dot{\theta}_1^2 \quad (19)$$

According to Eq. (16), the Jacobian terms describing $x_2(t)$ as a function of $x_1(t)$ and $\theta_1(t)$ can be taken directly from this relationship and are given by

$$\frac{\partial x_2}{\partial x_1}=-\frac{(l_0+x_2)\cos(\theta_1-\theta_2)+R\cos\theta_1}{l_0+x_2+R\cos\theta_2} \quad (20)$$

$$\frac{\partial x_2}{\partial\theta_1}=-\frac{1}{l_0+x_2+R\cos\theta_2}[R(l_0+x_2)\sin\theta_2$$
$$-(l_0+x_1)(l_0+x_2)\sin(\theta_1-\theta_2)-R(l_0+x_1)\sin\theta_1] \quad (21)$$

The Lagrangian equations of motion are given by

$$\frac{d}{dt}(\frac{\partial\mathcal{L}}{\partial\dot{x}_1})-[\frac{\partial\mathcal{L}}{\partial x_1}+\frac{\partial\mathcal{L}}{\partial x_2}(\frac{\partial x_2}{\partial x_1})]=0 \quad (22)$$

$$\frac{d}{dt}(\frac{\partial\mathcal{L}}{\partial\dot{\theta}_1})-[\frac{\partial\mathcal{L}}{\partial\theta_1}+\frac{\partial\mathcal{L}}{\partial x_2}(\frac{\partial x_2}{\partial\theta_1})]=0 \quad (23)$$

Substituting Eqs. (15), (20) and (21) into Eqs. (22) and (23) gives this kinematic motion

$$\ddot{x}_1+R\ddot{\theta}_1\sin\theta_1-(l_0+x_1)\dot{\theta}_1^2+g\cos\theta_1$$
$$+\omega_1^2[x_1-x_2\frac{(l_0+x_2)\cos(\theta_1-\theta_2)+R\cos\theta_1}{l_0+x_2+R\cos\theta_2}]=0 \quad (24)$$

$$[(l_0+x_1)^2+R^2+2R(l_0+x_1)\cos\theta_1]\ddot{\theta}_1+R\ddot{x}_1\sin\theta_1$$
$$+2(l_0+x_1+R\cos\theta_1)\dot{x}_1\dot{\theta}_1-(l_0+x_1)(g+R\dot{\theta}_1^2)\sin\theta_1$$
$$-\frac{\omega_1^2x_2}{l_0+x_2+R\cos\theta_2}[R(l_0+x_2)\sin\theta_2$$
$$-(l_0+x_1)(l_0+x_2)\sin(\theta_1-\theta_2)-R(l_0+x_1)\sin\theta_1]=0 \quad (25)$$

3. Ground reaction force

The vertical and horizontal ground reaction forces attributable to each limb can be calculated by recognizing that the line of action of each limb force points from the center of pressure to the center of mass (Fig. 6). Thus, the angle of the ground force vector φ_1 is given by

$$\varphi_1=\arctan\frac{(l_0+x_1)\sin\theta_1}{R+(l_0+x_1)\cos\theta_1} \quad (26)$$

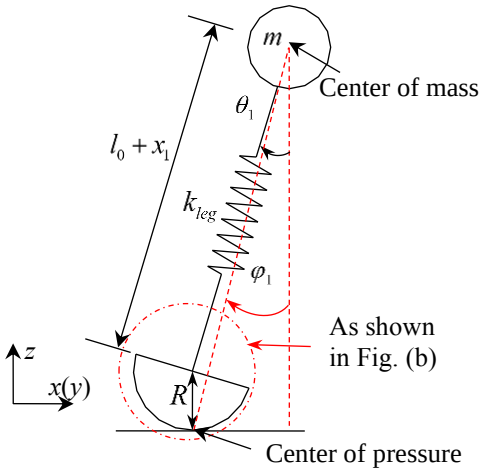

(a) Force diagram

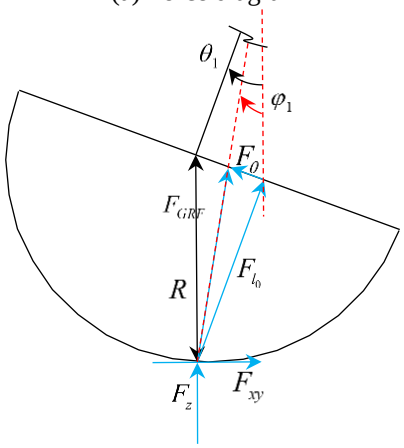

(b) Mechanical detail

Fig. 6 The ground reaction force

Knowing the spring force $F_{l_0}=k_{leg}x_1$ and the ground force vector, the circumferential force F_{θ_1} can be determined by

$$F_{\theta_1}=k_{leg}x_1\tan(\theta_1-\varphi_1) \quad (27)$$

The forces F_{l_0} and F_{θ_1} are then transformed into the ground reference frame to determine the forces in the horizontal (F_{xy}) and vertical (F_z) directions

$$F_z=\frac{k_{leg}x_1\cos\varphi_1}{\cos(\theta_1-\varphi_1)} \quad (28)$$

$$F_{xy}=\frac{k_{leg}x_1\sin\varphi_1}{\cos(\theta_1-\varphi_1)} \quad (29)$$

4. Parameter analysis

Given a set of model parameters, desired walking speed, and initial states (Fig. 7 with Θ being the impact angle), the Newmark-β method with γ=1/2 and β=1/4 was used to solve the above kinematic motion for studying the effects of

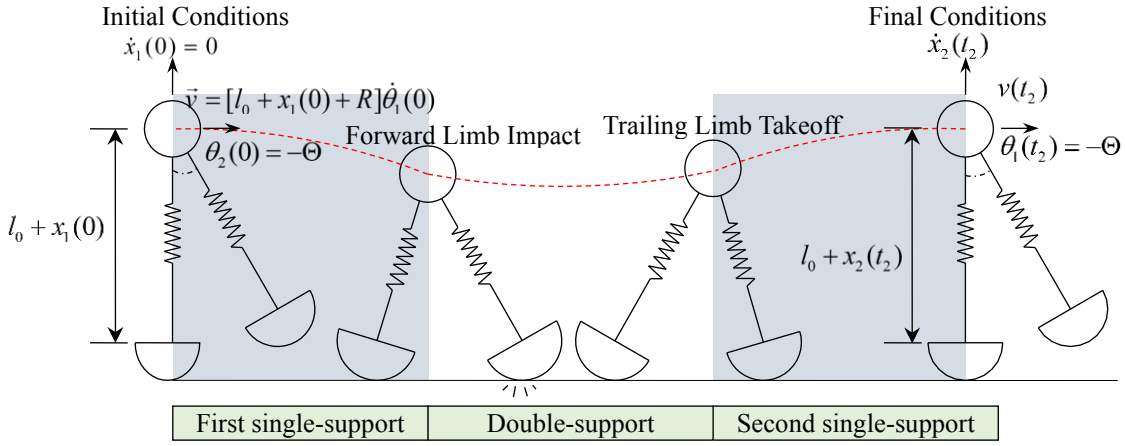

Fig. 7 A schematic diagram showing the whole simulation process

Table 2 The model parameters and desired walking speed

m (kg)	l_0 (m)	k_{leg} (kN/m)	Θ (rad)	v (m/s)
79	1	21	$-\pi/9$	1.35

Table 3 The duration time for each roller radius

Time	R (m)				
	0.10	0.15	0.20	0.25	0.30
FSS	0.2072	0.21325	0.21935	0.2254	0.2314
DS	0.54395	0.5578	0.5702	0.58235	0.5951
Total	0.95835	0.9843	1.0089	1.03315	1.0579
Percentage (%)	56.76	56.67	56.52	56.37	56.25

Note: 1. Total=2×First single support + Double support.
2. FSS represents first single support.
3. DS represents double support.
4. Percentage=Double support/Total time.

roller radius, stiffness, impact angle, and walking speed on the ground reaction force (horizontal load F_{xy}, and vertical load F_z), step length, energy transfer, and height of center of mass (HCOM) transfer. Note that the first and second single-support can be regarded as a reciprocal process, and only the first single-support and double-support are considered.

4.1 Effect of roller radius

The model parameters and desired walking speed are listed in Table 2, and the relationships between the roller radius and the ground reaction force, energy transfer, height of center of mass, and step length are shown in Fig. 8. The distribution of duration time for each roller radius is listed in Table 3, demonstrating that the duration time increases with the increasing roller radius, and the percentage for the double-support is approximately 56%. Fig. 8 shows that increasing the roller radius (while keeping other parameters constant) results in a decrease both in the peak of horizontal load F_{xy} and vertical load F_z at a fixed walking speed and virtually does not change the peak of HCOM. The rate of decrease for horizontal load F_{xy} is faster than vertical load F_z; and the inverted-pendulum model for walking is conservative such that there is no change in total energy. Increasing the roller radius results in a greater step length, with the change in excursion increasing approximately linearly with the roller radius.

4.2 Effect of stiffness

With the parameters fixed (Table 4) for the walking model, the model is feasible for walking at a fixed speed (v=1.35 m/s) with different stiffness (Fig. 9).

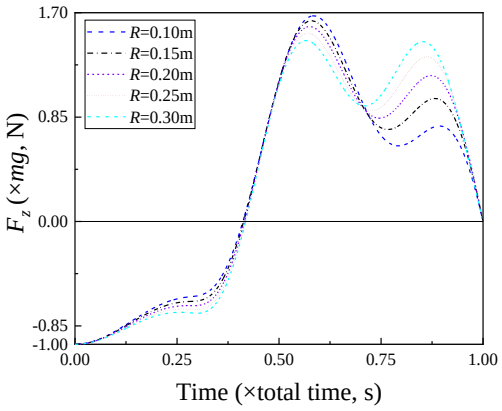

(a) F_z

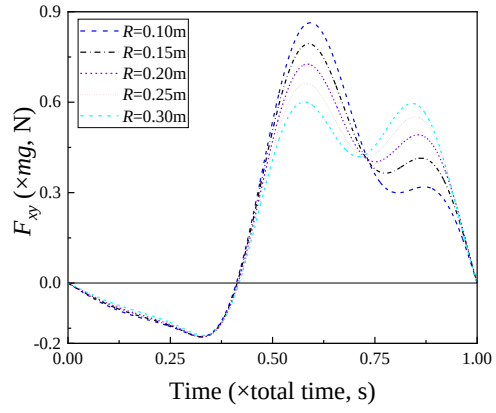

(b) F_{xy}

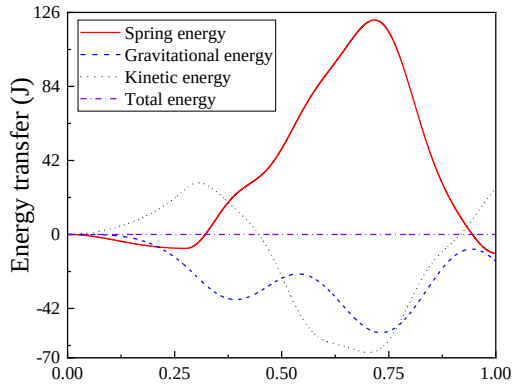

(c) Energy transfer (R=0.15m)

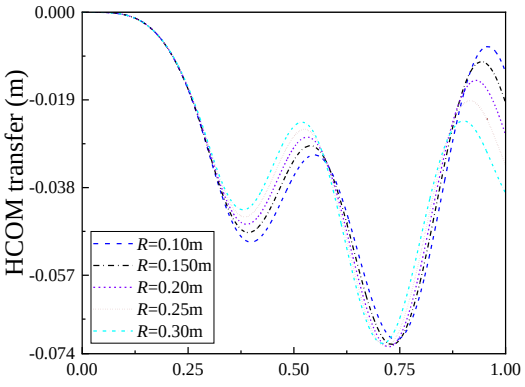

(d) Height of center of mass

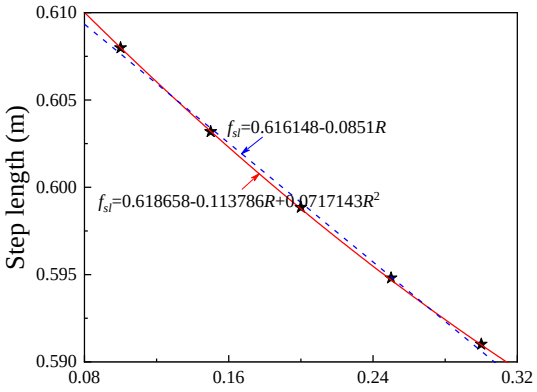

(e) Step length

Fig. 8 The effects of the roller radius

The duration time for each stiffness listed in Table 5 indicates that the effect on the double-support is significantly more apparent than the single-support, accounting for 50.27-60.50% as decreased with the increasing stiffness. From Fig. 9, the peak of both horizontal load F_{xy} and vertical load F_z are proportional to the stiffness, and the relationship on the HCOM excursion is just the reverse versus the ground reaction force. Similar to the roller radius effect, the inverted-pendulum model for walking is conservative such that there is no change in total energy. Increasing the stiffness results in greater step length excursion, and a fitting formula is shown in Fig. 9(e).

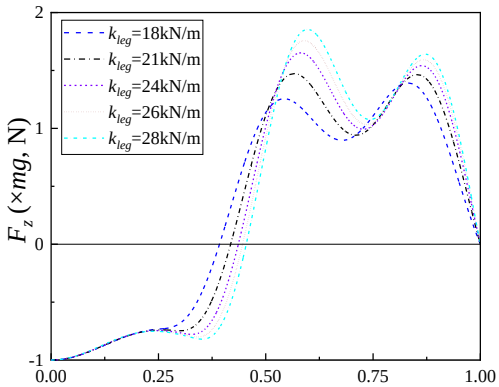

(a) F_z

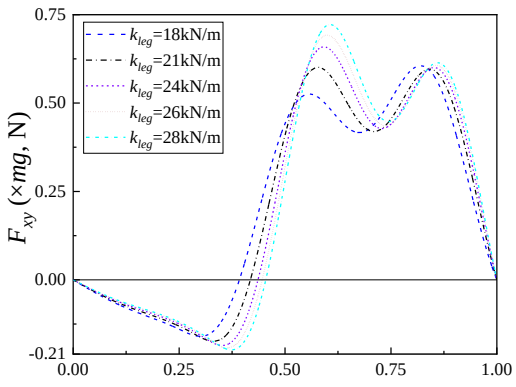

(b) F_{xy}

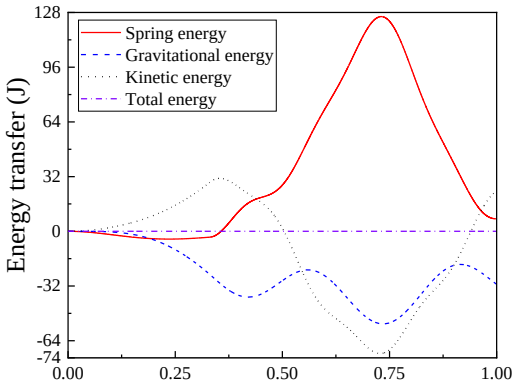

(c) Energy transfer (k_{leg}=28kN/m)

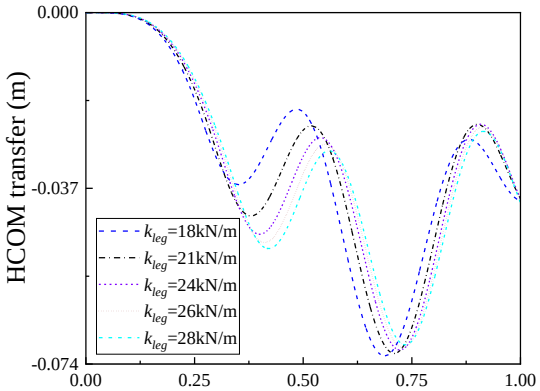

(d) Height of center of mass

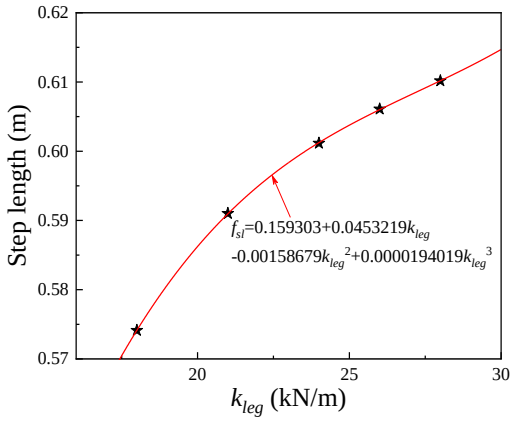

(e) Step length

Fig. 9 The effects of stiffness

Table 4 The parameters of walking model

m (kg)	l_0 (m)	R (m)	Θ (rad)
79	1	0.3	-π/9

Table 5 The distribution of duration time for each stiffness

Time	k_{leg} (kN/m)				
	18	21	24	26	28
FSS	0.2168	0.2314	0.2401	0.2443	0.24775
DS	0.66405	0.5951	0.5479	0.5227	0.50095
Total	1.09765	1.0579	1.0281	1.0113	0.99645
Percentage (%)	60.50	56.25	53.29	51.69	50.27

Table 6 The parameters of the walking model for the impact angle effect

m (kg)	l_0 (m)	R (m)	v (m/s)	k_{leg} (kN/m)
79	1	0.3	1.35	21

Table 7 The distribution of duration time for each impact angle

Time	Θ (rad)				
	-π/10	-19π/180	-π/9	-7π/60	-11π/90
FSS	0.1897	0.21205	0.2314	0.249	0.26545
DS	0.7931	0.6325	0.5951	0.57365	0.5568
Total	1.1725	1.0566	1.0579	1.07165	1.0877
Percentage (%)	67.64	59.86	56.25	53.53	51.19

4.3 Effect of impact angle

Considering the quantitative parameters listed in Table 6, the variation of impact angle significantly affects the vertical load F_z, horizontal load F_{xy}, and duration time. An increasing impact angle gives a substantial decrease and increase in peaks of F_z (Fig. 10(a)), F_{xy} (Fig. 10(b)) and HCOM transform, respectively. The duration time listed in Table 7 demonstrates that the duration time of double-support is the main affecting parameter, accounting for

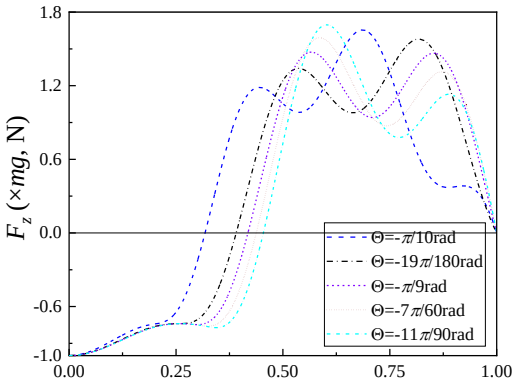

(a) F_z

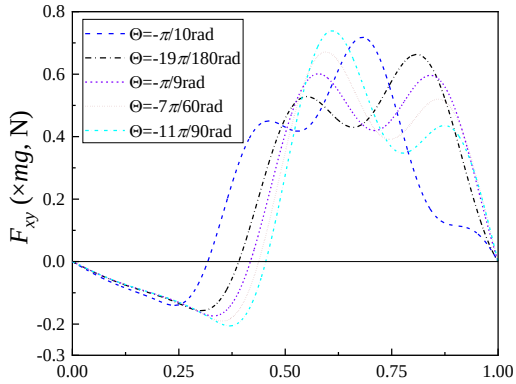

(b) F_{xy}

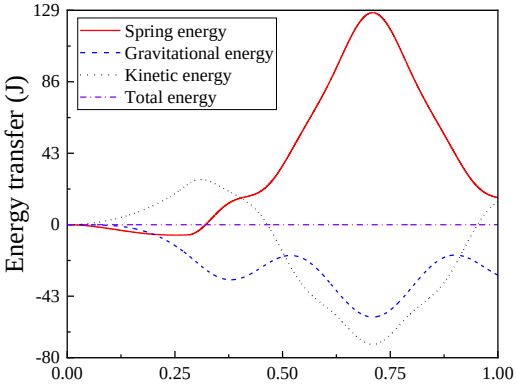

(c) Energy transfer (Θ =-π/9rad)

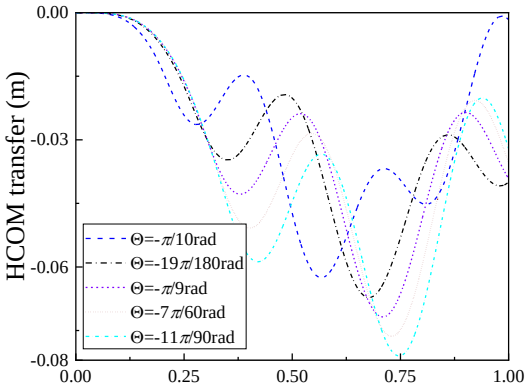

(d) Height of center of mass

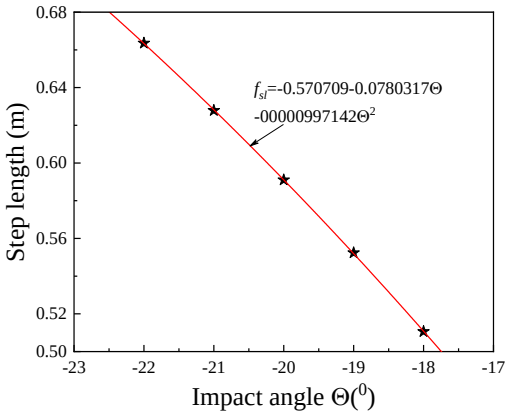

(e) Step length

Fig. 10 The effects of impact angle

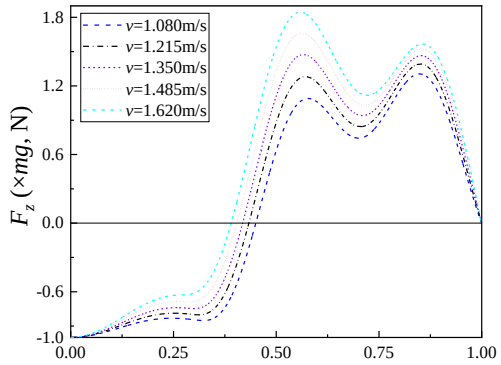

(a) F_z

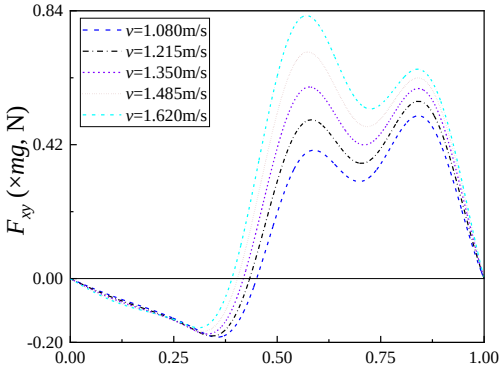

(b) F_{xy}

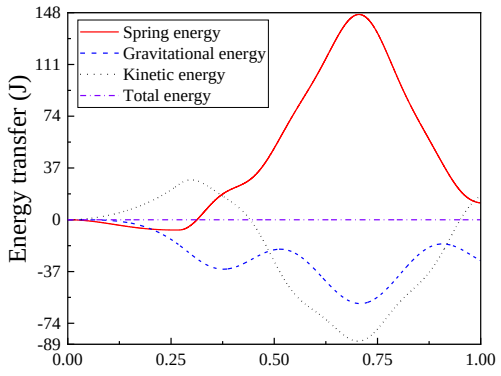

(c) Energy transfer (v=1.485m/s)

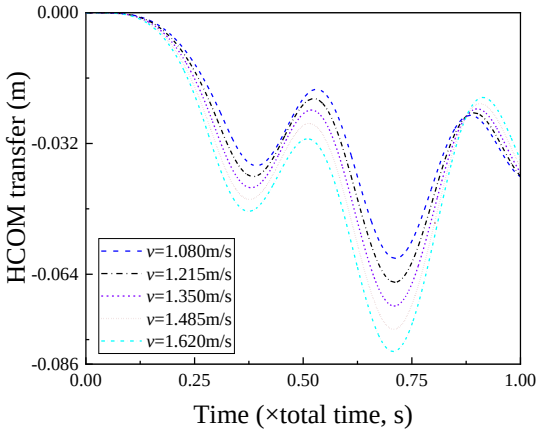

(d) Height of center of mass

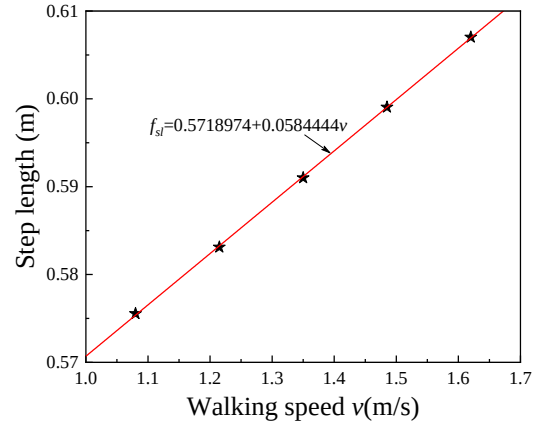

(e) Step length

Fig. 11 The effects of walking speed

51.19-67.64%. Similar to the roller radius and stiffness effects, the inverted-pendulum model for walking is conservative such that there is no change in total energy. Increasing the impact angle results in a greater step length, with the change in excursion increasing approximately linearly with the impact angle.

4.4 Effect of walking speed

Based on the set parameters listed in Table 8, the walking effect on the vertical load F_z, horizontal load F_{xy}, energy transfer, and HCOM transfer are shown in Fig. 11. From the figure, it can be seen that the loads F_z and F_{xy}, HCOM transfer, and step length all increase with the progressive walking speed, and the change rate increases approximately linearly with the walking speed. For the duration time (including first single-support, double-support, and total time), the relationship is contrary to the above conclusion, and the range is 53.24-58.53%. There is still no change in the total energy for walking speed.

4.5 Relation curve

For the convenience of getting the peak of the ground reaction force which can been used to calculate the peak acceleration a_p induced by human walking according to Eq. (30) (Murray *et al*. 1997, 2016),

$$a_p = \frac{P_0 g e^{-0.35 f_n}}{\xi W} \tag{30}$$

where P_0 is the amplitude of the vertical force, g is the gravitational acceleration, f_n is the structure's natural frequency, W is the effective weight of the structure, and ξ is damping ratio. Fig. 12 shows the fitted curves between the peak ground reaction force and each influencing parameter (i.e., roller radius, stiffness, impact angle, and walking speed.

Table 8 The parameters of the walking model for the walking speed effect

m (kg)	l_0 (m)	k_{leg} (kN/m)	R (m)	Θ (m/s)
79	1	21	0.3	-π/9

Table 9 The distribution of duration time for each walking speed

Time	v (m/s)				
	1.08	1.215	1.35	1.485	1.62
FSS	0.2668	0.2472	0.2314	0.21835	0.20725
DS	0.60745	0.60085	0.5951	0.5899	0.5851
Total	1.14105	1.09525	1.0579	1.0266	0.9996
Percentage (%)	53.24	54.86	56.25	57.46	58.53

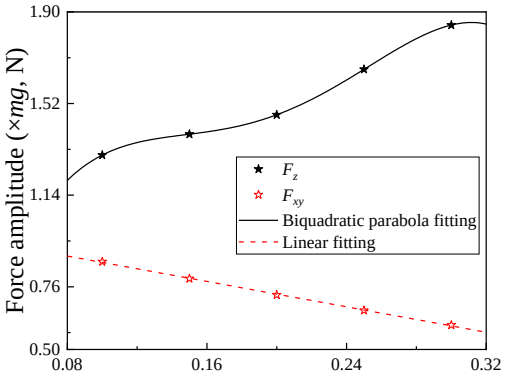

(a) Roller radius

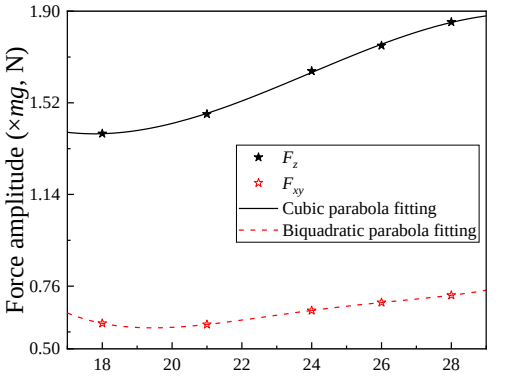

(b) Stiffness

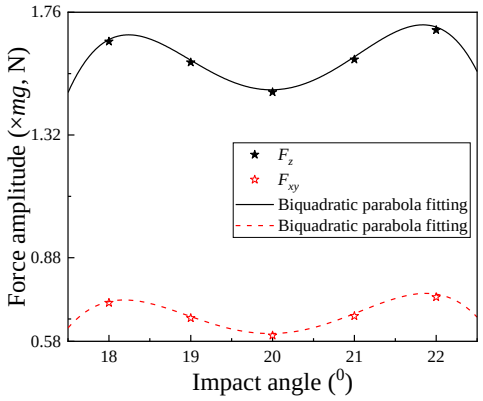

(c) Impact angle

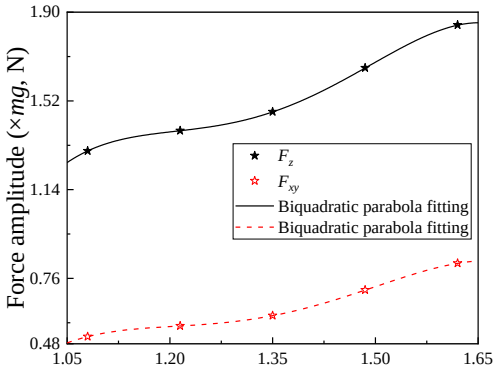

(d) Walking speed

Fig. 12 Relation curve between force amplitude and influencing parameters

5. Dynamical load factor (DLF)

Similar to the current research (Avossa *et al*. 2017; Peng *et al*. 2015; Younis *et al*. 2017), only the ground reaction force of double-support phase is considered. The proposed walking formula for vertical force F_z is expressed by

$$F_z(t) = G[\alpha_{w0} + \sum_{i=1}^{n} \alpha_{wi} \sin(2i\pi f_w t - \theta_{wi})] \tag{31}$$

where the coefficients are calculated by

$$\alpha_{w0} = \frac{1}{T}\int_{t_0}^{t_0+T} f_w(t)dt \tag{32}$$

$$a_i = \frac{2}{T}\int_{t_0}^{t_0+T} f_w(t)\cos i\omega t dt \tag{33}$$

$$b_i = \frac{2}{T}\int_{t_0}^{t_0+T} f_w(t)\sin i\omega t dt \tag{34}$$

$$\alpha_{wi} = \sqrt{a_i^2 + b_i^2} \tag{35}$$

$$\theta_{wi} = -\arctan\frac{a_i}{b_i} \tag{36}$$

Table 10, Table 11, Table 12 and Table 13 summarize the coefficients α_{wi} and θ_{wi} for each parameter, respectively.

Table 10 The coefficients α_{wi} and θ_{wi} for each roller radius

	R (m)				
	0.10	0.15	0.20	0.25	0.30
f_w (Hz)	1.84	1.79	1.75	1.72	1.68
α_{w0}	0.655	0.692	0.720	0.738	0.748
α_{w1}	0.782	0.757	0.722	0.735	0.796
α_{w2}	0.505	0.558	0.586	0.615	0.633
α_{w3}	0.108	0.108	0.122	0.113	0.072
θ_{w1}	$1/5\pi$	$3/20\pi$	$7/100\pi$	$2/50\pi$	$1/25\pi$
θ_{w2}	$-2/50\pi$	0	$-2/50\pi$	$-2/125\pi$	$2/25\pi$
θ_{w3}	$2/5\pi$	$2/5\pi$	$7/25\pi$	$7/25\pi$	$2/5\pi$

Table 11 The coefficients α_{wi} and θ_{wi} for each stiffness

	k_{leg} (kN/m)				
	18	21	24	26	28
f_w (Hz)	1.51	1.68	1.83	1.91	2.00
α_{w0}	0.669	0.748	0.820	0.866	0.911
α_{w1}	0.766	0.796	0.837	0.866	0.897
α_{w2}	0.554	0.633	0.692	0.725	0.753
α_{w3}	0.049	0.072	0.087	0.094	0.102
θ_{w1}	$3/20\pi$	$1/25\pi$	$-1/25\pi$	$-1/10\pi$	$-7/50\pi$
θ_{w2}	$9/25\pi$	$2/25\pi$	$-3/25\pi$	$-1/4\pi$	$-9/25\pi$
θ_{w3}	$-7/25\pi$	$2/5\pi$	$1/10\pi$	$-7/100\pi$	$-6/25\pi$

Table 12 The coefficients α_{wi} and θ_{wi} for each impact angle

	Θ (rad)				
	$-\pi/18$	$-\pi/12$	$-\pi/9$	$-7\pi/60$	$-11\pi/90$
f_w (Hz)	1.26	1.58	1.68	1.74	1.80
α_{w0}	0.684	0.742	0.748	0.735	0.711
α_{w1}	0.854	0.837	0.796	0.782	0.797
α_{w2}	0.220	0.578	0.633	0.647	0.641
α_{w3}	0.331	0.027	0.072	0.101	0.118
θ_{w1}	$9/20\pi$	$7/50\pi$	$1/25\pi$	$-1/100\pi$	$-1/20\pi$
θ_{w2}	$-1/25\pi$	$19/50\pi$	$2/25\pi$	$-3/20\pi$	$-9/25\pi$
θ_{w3}	$-1/25\pi$	$1/25\pi$	$2/5\pi$	$1/10\pi$	$-17/180\pi$

Table 13 The coefficients α_{wi} and θ_{wi} for each walking speed

	v (m/s)				
	1.08	1.215	1.35	1.485	1.62
f_w (Hz)	1.65	1.66	1.68	1.70	1.71
α_{w0}	0.550	0.650	0.748	0.845	0.939
α_{w1}	0.748	0.771	0.796	0.822	0.851
α_{w2}	0.571	0.606	0.633	0.653	0.665
α_{w3}	0.063	0.066	0.072	0.079	0.086
θ_{w1}	$-1/10\pi$	$-3/125\pi$	$1/25\pi$	$1/10\pi$	$4/25\pi$
θ_{w2}	$-2/25\pi$	0	$2/25\pi$	$3/20\pi$	$1/5\pi$
θ_{w3}	$-1/50\pi$	$1/5\pi$	$2/5\pi$	$-9/20\pi$	$-11/60\pi$

6. Conclusions

A comprehensive research project was undertaken to study the human walking load based on the inverted-pendulum model which consists of a point supported by spring limbs with roller feet. Based on the study results, the following conclusions are offered:

• The inverted-pendulum model for walking is conservative as there is no change in total energy.

• The duration time increases with the increasing roller radius. The increasing roller radius results in a decrease in peaks of horizontal load F_{xy}, vertical load F_z, and step length at a fixed walking speed and virtually does not change the peak of HCOM.

• Both the peaks of horizontal load F_{xy} and vertical load F_z and the step length are proportional to the stiffness, while the conclusion on the HCOM excursion is just the reverse versus the ground reaction force.

• An increasing impact angle results in abrupt change in the peak of vertical load F_z, horizontal load F_{xy}, step length and HCOM transform.

• The vertical load F_z, horizontal load F_{xy}, HCOM transfer, and step length all increase with the progressive walking speed.

• The duration time of double-support phase accounts for approximately 50-70% of the total time.

Acknowledgments

The authors are grateful for the financial support provided by Fundamental Research Funds for the Central Universities (Grant No. cqu2018CDHB1A08) and National Natural Science Foundation of China (Grant No. 51622802, 51438001).

References

Ahmadi, E., Caprani, C., Zivanovic S. and Heidarpour, A. (2018), "Vertical ground reaction forces on rigid and vibrating surfaces for vibration serviceability assessment of structures", *Eng. Struct.*, **172**, 723-738. https://doi.org/10.1016/j.engstruct.2018.06.059.

Allen, D.E. and Murray, T.M. (1993), "Design criterion for vibrations due to walking", *Eng. J.* AISC, **30**(4), 117-129.

Avossa, A.M., Demartino, C. and Ricciardelli, F. (2017), "Design procedures for footbridges subjected to walking loads: comparison and remarks", *Balt. J. Road Bridge E.*, **12**(2), 94-105.

Bachmann, H. and Ammann, W. (1987), *Vibrations in Structures Induced by Man and Machines*, International Association for Bridge and Structural Engineering, Zurich, Switzerland.

Blanchard, J., Davies, B.L. and Smith, J.W. (1977), "Design criteria and analysis for dynamic loading of footbridges", *Proceeding of a Symposium on Dynamic Behaviour of Bridges at the Transport and Road Research Laboratory*, Berkshire, England, May.

Bocian, M., Macdonald, J.H.G. and Burn, J.F. (2014), "Probabilistic criteria for lateral dynamic stability of bridges under crowd loading", *Comput. Struct.*, **136**, 108-119. https://doi.org/10.1016/j.compstruc.2014.02.003.

Brownjohn, J.M.W., Chen, J., Bocian, M., Racic, V. and Shahabpoor, E. (2018), "Using inertial measurement units to identify medio-lateral ground reaction forces due to walking and

swaying", *J. Sound Vib.*, **426**, 90-110. https://doi.org/10.1016/j.jsv.2018.04.019.
Cao, L., Liu, J.P., Zhou, X.H. and Chen, Y.F. (2018), "Vibration performance characteristics of a long-span and light-weight concrete floor under human-induced loads", *Struct. Eng. Mech.*, **65**(3), 349-357. https://doi.org/10.12989/sem.2018.65.3.349.
Chen, J., Peng, Y.X. and Ye, T. (2013), "On methods for extending a single footfall trace into a continuous force curve for floor vibration serviceability analysis", *Struct. Eng. Mech.*, **46**(3), 179-196. https://doi.org/10.12989/sem.2013.46.2.179.
Chen, J., Wang, H.Q. and Peng, Y.X. (2014), "Experimental investigation on Fourier-series model of walking load and its coefficients", *J. Vib. Shock*, **33**(8), 11-15.
Davis, B. and Avci, O. (2015), "Simplified vibration serviceability evaluation of slender monumental stairs", *J. Struct. Eng.*, **141**(11), https://doi.org/10.1061/(ASCE)ST.1943-541X.0001256.
Han, H.X., Zhou, D. and Ji, T.J. (2017), "Mechanical parameters of standing body and applications in human-structure interaction", *Int. J. Appl. Mech.*, **9**(2). https://doi.org/10.1142/S1758825117500211.
Kerr, S.C. (1998), "Human induced loading on staircases", Ph.D. Dissertation, University College London, London.
Kim, J.H. and Jeon, J.Y. (2014), "Effects of vibration characteristics on the walking discomfort of floating floors on concrete slabs", *J. Acoust. Soc. AM.*, **136**(4), 1702-1711. https://doi.org/10.1121/1.4894686.
Liu, J.P., Cao, L. and Chen, Y. F. (2019), "Vibration performance of composite steel-bar truss slab with steel girder", Steel Compos. Struct., **30**(6), 577-589. https://doi.org/10.12989/scs.2019.30.6.577.
Mello, A.V.A., da Silva, J.G.S., da S. Vellasco, P.C.G., de Andrade, S.A.L. and de Lima, L.R.O. (2008), "Dynamic analysis of composite systems made of concrete slabs and steel beams", *J. Constr. Steel Res.*, **64**, 1142-1151. https://doi.org/10.1016/j.jcsr.2007.09.011.
Murray, T.M., Allen, D.E. and Ungar, E.E. (1997), *Floor Vibrations Due to Human Activity*, American Institute of Steel Construction, Inc., Chicago, USA.
Murray, T.M., Allen, D.E., Ungar, E.E. and Davis, D.B. (2016), *Vibrations of Steel-Framed Structural Systems Due to Human Activity* (2nd Edition), American Institute of Steel Construction, Inc., Chicago, USA.
Peng, Y.X., Chen, J. and Ding, G. (2015), "Walking load model for single footfall trace in three dimensions based on gait experiment", *Struct. Eng. Mech.*, **54**(5), 937-953. https://doi.org/10.12989/sem.2015.54.5.937.
Petrovic-Kotur, S.P. and Pavic, A.P. (2016), "Vibration analysis and FE model updating of lightweight steel floors in full-scale prefabricated building", *Struct. Eng. Mech.*, **58**(2), 277-300. https://doi.org/10.12989/sem.2016.58.2.277.
Rainer, J.H., Pernica, G. and Allen, D.E. (1988), "Dynamic loading and response of footbridges", *Can. J. Civil. Eng.*, **15**(1), 66-71. https://doi.org/10.1139/l88-007.
Setareh, M. (2016), "Vibration serviceability issues of slender footbridges", *J. Bridge Eng.*, **21**(11), https://doi.org/10.1061/(ASCE)BE.1943-5592.0000951.
Setareh, M. and Gan, S.Q. (2018), "Vibration testing, analysis, and human-structure interaction studies of a slender footbridge", *J. Perform. Constr. Fac.*, **32**(5), https://doi.org/10.1061/(ASCE)CF.1943-5509.0001213.
Smith, A.L., Hicks, S.J. and Devine, P.J. (2009), *Design of Floors for Vibration*: *A New Approach*, The Steel Construction Institute, Berkshire, United Kingdom.
Van Nimmen, K., Lombaert, G., De Roeck, G. and Van den Broeck, P. (2017), "The impact of vertical human-structure interaction on the response of footbridges to pedestrian excitation", *J. Sound Vib.*, **402**, 104-121. https://doi.org/10.1016/j.jsv.2017.05.017.
Wang, J. and Chen, J. (2017), "A comparative study on different walking load models", *Struct. Eng. Mech.*, **63**(6), 847-856. https://doi.org/10.12989/sem.2017.63.6.847.
Whittington, B.R. and Thelen, D.G. (2009), "A simple mass-spring model with roller feet can induce the ground reactions observed in human walking", J. Biomech. Eng., **131**(1). https://doi.org/10.1115/1.3005147.
Yin, S.H. (2017), "Pedestrian-induced vibration of a simply-supported beam", *J. Mech.*, **33**(5), 577-591. https://doi.org/10.1017/jmech.2016.94.
Young, P. (2001), "Improved floor vibration prediction methodologies", *Proceedings of Arup Vibration Seminar on Engineering for Structure Vibration-Current Developments in Research and Practice*, London, October.
Younis, A., Avci, O., Hussein, M., Davis, B. and Reynolds, P. (2017), "Dynamic forces induced by a single pedestrian: a literature review", *Appl. Mech. Rev.*, **69**(2). https://doi.org/10.1115/1.4036327.
Zhou, X.H., Liu, J.P., Cao, L. and Li, J. (2017), "Vibration serviceability of pre-stressed concrete floor system under human activity", *Struct. Infrastruct. E.*, **13**(8), 967-977. https://doi.org/10.1080/15732479.2016.1229796.

CC